Nuclear Instruments and Methods in Physics Research A 829 (2016) 367–371

Contents lists available at ScienceDirect

Nuclear Instruments and Methods in Physics Research A

journal homepage: www.elsevier.com/locate/nima

Efficient numerical modelling of the emittance evolution of beams with finite energy spread in plasma wakefield accelerators

T.J. Mehrling [a,*], R.E. Robson [b], J-H. Erbe [a], J. Osterhoff [a]

[a] Deutsches Elektronen-Synchrotron DESY, 22607 Hamburg, Germany
[b] Centre for Quantum Dynamics, School of Natural Sciences, Griffith University, Brisbane, Australia

ARTICLE INFO

Available online 6 February 2016

Keywords:
Plasma wakefield acceleration
Numerical modeling
Emittance
Particle-in-cell

ABSTRACT

This paper introduces a semi-analytic numerical approach (SANA) for the rapid computation of the transverse emittance of beams with finite energy spread in plasma wakefield accelerators in the blowout regime. The SANA method is used to model the beam emittance evolution when injected into and extracted from realistic plasma profiles. Results are compared to particle-in-cell simulations, establishing the accuracy and efficiency of the procedure. In addition, it is demonstrated that the tapering of vacuum-to-plasma and plasma-to-vacuum transitions is a viable method for the mitigation of emittance growth of beams during their injection and extraction from and into plasma cells.

1. Introduction

Breakthroughs such as the demonstration of the energy doubling of 42 GeV electrons within a distance of less than a meter [1] established the credentials of plasma wakefield accelerators (PWFA) [2,3] as a viable future compact and affordable alternative to current conventional accelerators. In this plasma-based accelerator approach, a highly relativistic, high current *drive beam*, traverses a plasma target and thereby excites a large amplitude plasma wave. A *witness beam*, either externally injected or formed from plasma electrons by means of an internal injection method, is accelerated by virtue of the fields in the wake of the drive beam.

The increasing scientific interest in PWFAs eventually led to advances such as the experimental acceleration of distinct electron beams with high efficiency [4], and is primarily associated with the remarkable capability of these accelerators to generate and sustain extreme accelerating wakefields in excess of $\sim 10\,\mathrm{GV/m}$ during drive beam propagation in plasmas over meter-scale distances without substantial dephasing between drive and witness beam. This feature renders PWFAs an attractive technology candidate for the compact generation of brilliant X-rays or even for future compact and affordable particle colliders [5]. Besides the demands for high beam energies, these applications entail stringent requirements with regard to the beam quality. While a number of numerical studies [6–11] indicated the potential of PWFAs to generate high quality beams, one of the major challenges constitutes the preservation of these qualities during the witness beam extraction and transport to the interaction region. In addition, the beams may have to be transported in between successive plasma sections and re-injected without significant quality deterioration in staged acceleration concepts, such as proposed e.g. in [5].

As shown in previous works [12,13], the *transverse phase space emittance*, which is a figure of merit for the transverse beam quality, grows during the injection and propagation in a plasma target if beams are not matched appropriately. In addition, the phase space emittance of beams with finite energy spread and significant divergence may increase dramatically during the expansion in the vacuum downstream the plasma target [14,15]. The challenges to match beams into the plasma as well as to extract them can be substantially mitigated and the quality deterioration suppressed by the use of tapered vacuum-to-plasma and plasma-to-vacuum transitions, respectively, as indicated by several studies [13,16–19]. The rigorous investigation of the beam injection and extraction processes in PWFA typically involves the use of particle-in-cell (PIC) simulations. However, for the realisation of parameter scans e.g. for the optimisation of the beam parameters or of the plasma density profile, such an approach is inappropriately time consuming and computationally highly demanding.

This paper presents an alternative, computationally efficient semi-analytic numerical approach (SANA) for the investigation of the emittance evolution of beams with finite energy spread in PWFAs. Such an approach allows for the rapid optimisation of beam parameters and the longitudinal plasma profile in terms of the beam quality transport. This method was outlined in [20] and

* Corresponding author.
E-mail address: timon.mehrling@desy.de (T.J. Mehrling).

http://dx.doi.org/10.1016/j.nima.2016.01.091
0168-9002/

is generalised in the present work to model beams with varying energy and energy spread. Section 2 reviews the physical basis and the moment procedure, and introduces the mathematical formulation of the semi-analytic numerical approach. The procedure is thereafter applied to a scenario in PWFA in Section 3. Results are compared to those obtained from PIC simulations with the 3D quasi-static code HiPACE [21] to establish the accuracy and efficiency of the procedure. In addition, this physical showcase study demonstrates the effectiveness of such realistic plasma profiles to mitigate the emittance growth during the injection and propagation in the plasma target and during the extraction. The paper is finalised with a summary and conclusion.

2. Mathematical model

2.1. Physical basis and moment procedure

The witness electron beam considered in the following propagates in positive z-direction in a plasma wakefield in the blowout regime excited by a drive beam. The witness beam particles are highly relativistic in axial direction and non- to mildly relativistic in the transverse direction i.e. $p_z \simeq \gamma \gg 1$, where γ is the Lorentz factor and p_z is the axial momentum normalised to $m_e c$. The beam particle phase space distribution function, which is in the following assumed to be symmetric in x and p_x with respect to zero, may therefore be characterised by $f = f(x, p_x, \zeta, \gamma; t)$. Here, t is the time normalised with respect to the inverse of a reference plasma density $\omega_{p,0}^{-1}$. The transverse particle offset coordinate x, the propagation axis coordinate z and the co-moving coordinate $\zeta = z - t$ are normalised to $k_{p,0}^{-1} = c/\omega_{p,0}$. The transverse momentum, denoted by p_x is given in units of $m_e c$. The temporal evolution of this particle distribution is prescribed by the *Vlasov equation* [22] which, in a manner similar to that described in Ref. [20], can be written to a good approximation as

$$(\partial_t + p_x/\gamma \partial_x + \partial_{p_x} F_x + \partial_\gamma F_z) f = 0 \tag{1}$$

where F_x and F_z are the transverse and longitudinal forces imposed onto the beam particles, normalised to $\omega_{p,0}\, m_e c$. The co-moving position hereby is assumed invariant, which is a good approximation for scenarios in PWFA where the slippage of witness beam electrons with respect to the speed of light frame over the regarded acceleration distance is typically negligible. Within the blowout of plasma waves, the transverse force is a function of the transverse coordinate and time $F_x = F_x(x, t)$ and the longitudinal force is a function of the co-moving position and time $F_z = F_z(\zeta, t)$ (compare e.g. [23]).

The aim is to compute the transverse phase space emittance

$$\epsilon = \sqrt{\langle x^2 \rangle \langle p_x^2 \rangle - \langle x p_x \rangle^2} \tag{2}$$

in an economical way. The averages $\langle \ldots \rangle$ are defined by

$$\langle \Phi(x, p_x, \zeta, \gamma) \rangle(t) = \frac{1}{N} \int dx \int dp_x \int d\zeta \int d\gamma\, \Phi f \tag{3}$$

in terms the particle number density f. The particle number is calculated via

$$N = \int dx \int dp_x \int d\zeta \int d\gamma, f. \tag{4}$$

While knowledge of f is essential for a complete picture of the electron bunch in phase space, an analytic solution of (1) is generally not possible. Finding numerical approximations for the distribution function f which satisfy the Vlasov equation e.g. by means of direct Vlasov solvers (see, e.g. [24–26]) or by means of PIC simulations (see, e.g. [27–29]) can be both computationally demanding and time-consuming.

However, if only *averages* such as in (2) are required then, as explained in [20], there is an alternative, computationally economical procedure, which yields these quantities *directly*, without the need to find the f first. Instead of solving for f in the Vlasov equation, one can multiply the Vlasov equation with Φ and then perform an integration by parts over the phase space variables, yielding the general moment equation [20]

$$\partial_t \langle \Phi \rangle = \langle p_x/\gamma \partial_x \Phi \rangle + \langle F_x\, \partial_{p_x} \Phi \rangle + \langle F_z\, \partial_\gamma \Phi \rangle. \tag{5}$$

As explained in [20] this *moment procedure* [30] generally yields an infinite chain of equations which, like for fluid models in configuration space, must be truncated via some Ansatz.

The transverse field within the blowout cavity depends linearly on the transverse offset to the propagation axis, $F_x(x, t) = -\hat{k}_x(t) x$. This allows us to express the equations for the phase space moments of interest, here $\Phi = \{x^2, x p_x, p_x^2, \gamma\}$, as

$$\partial_t \langle x^2 \rangle = 2 \langle x p_x/\gamma \rangle \tag{6}$$

$$\partial_t \langle x p_x \rangle = \langle p_x^2/\gamma \rangle - \hat{k}_x \langle x^2 \rangle \tag{7}$$

$$\partial_t \langle p_x^2 \rangle = -2 \hat{k}_x \langle x p_x \rangle \tag{8}$$

$$\partial_t \langle \gamma \rangle = \langle F_z \rangle. \tag{9}$$

For *mono-energetic beams,* this set of equations is closed and may be related to the well known beam envelope equations [31]. However, the present paper goes beyond these envelope models, and investigates the transverse dynamics of realistic beams with non-zero, variable correlated or uncorrelated energy spread, and a variable energy.

2.2. Semi-analytical numerical approach

The following generalises the method introduced in [20] to solve the more comprehensive set of Eqs. (6)–(9). The basis of this method is the discretisation of the distribution function according to

$$f(x, p_x, \zeta, \gamma; t) \simeq \sum_{k=1}^{M} N_k \delta(\gamma - \gamma_k(t)) \delta(\zeta - \zeta_k) f_k(x, p_x; t) \tag{10}$$

where M is the number of mono-energetic subsets, N_k is the invariant number of electrons in one subset, $\gamma_k(t)$ is the time-dependent Lorentz factor of an energy subset and $f_k(x, p_x)$ is the normalised subset transverse phase space distribution function. It should be noted that γ here is an Eulerian phase-space quantity while $\gamma_k(t)$ is a Lagrangian quantity. The discretised distribution function (10) allows for the modelling of beams with correlated and uncorrelated energy spread. The total particle number is in this context given by

$$N = \sum_{k=1}^{M} N_k. \tag{11}$$

The co-moving position of a subset is hereby assumed invariable in compliance with the basic assumptions for the Vlasov equation (1).

The phase space quantities of interest for the study on the quality evolution of beams are separable $\Phi(x, p_x, \zeta, \gamma) = \Phi_t(x, p_x) \cdot \Phi_l(\zeta, \gamma)$, and the according phase space averages can thus be formed as follows:

$$\begin{aligned}
\langle \Phi(x, p_x, \zeta, \gamma) \rangle &= \frac{1}{N} \int dx dp_x d\zeta d\gamma \Phi(x, p_x, \zeta, \gamma) f(x, p_x, \zeta, \gamma; t) \\
&= \frac{1}{N} \int dx\, dp_x d\zeta\, d\gamma \Phi_t(x, p_x) \Phi_l(\zeta, \gamma) f(x, p_x, \zeta, \gamma; t) \\
&= \frac{1}{N} \sum_{k=1}^{M} N_k \langle \Phi_l(\zeta, \gamma) \rangle_k \int dx\, dp_x\, \Phi_t(x, p_x) f_k(x, p_x; t) \\
&= \frac{1}{N} \sum_{k=1}^{M} N_k \langle \Phi_l(\zeta, \gamma) \rangle_k \cdot \langle \Phi_t(x, p_x) \rangle_k.
\end{aligned} \tag{12}$$

Phase space averages may hence be expressed as a sum over the product of *longitudinal averages*

$$\langle \Phi_l(\zeta,\gamma)\rangle_k = \Phi_l(\zeta_k,\gamma_k) \tag{13}$$

and *transverse averages*

$$\langle \Phi_t(x,p_x)\rangle_k = \int dx \int dp_x \Phi_t(x,p_x) f_k(x,p_x;t) \tag{14}$$

of elements of the discretised particle distribution function $f(x,p_x,\zeta,\gamma;t)$. This allows for the formulation of the transverse moment equations for a particle subset according to

$$\partial_t \langle x^2\rangle_k = 2\langle x p_x\rangle_k/\gamma_k \tag{15}$$

$$\partial_t \langle x p_x\rangle_k = \langle p_x^2\rangle_k/\gamma_k - \hat{k}_x(t)\langle x^2\rangle_k \tag{16}$$

$$\partial_t \langle p_x^2\rangle_k = -2\hat{k}_x(t)\langle x p_x\rangle_k \tag{17}$$

$$\partial_t \gamma_k = F_z(\zeta_k,t). \tag{18}$$

This set of equations is closed and the phase space moments $\langle \Phi(x,p_x,\zeta,\gamma)\rangle$ can now be formed according to Eq. (12) after the numerical or analytical calculation of Eqs. (15)–(18).

3. Physical studies

The mathematical model described in Section 2 will now be applied to the following scenario in PWFA. A drive beam propagates into a plasma target and excites a plasma wave in the blowout regime. Trailing to the drive beam, at a fixed distance is a witness beam, which is accelerated by virtue of the longitudinal plasma wakefield during the process. Both beams exit the plasma target and subsequently propagate through vacuum downstream of the plasma. The witness beam initially has a significant energy spread. During the propagation in the plasma, electrons in the beams perform *betatron oscillations* with frequency $\omega_\beta = \omega_p/\sqrt{2\gamma_e}$ (cf. e.g. [32]). This frequency depends on the individual electron energy γ_e as well as on the local plasma frequency $\omega_p(z) = \sqrt{4\pi n(z) e^2/m_e}$. Two longitudinal profiles for the plasma target are considered in the following, a *standard profile* and a *tailored profile* (see Fig. 1). The former represents a typical case for plasma cells with vacuum-to-plasma and plasma-to-vacuum interfaces rising and falling rapidly compared to the local *betatron wavelength* $\lambda_\beta \simeq 2\pi c/\omega_\beta$. The latter was shaped in order to enable a release of the beam from the plasma cell to vacuum with the betatron frequency changing quasi-adiabatically. Previous works showed that plasma-to-vacuum transitions which are long compared to the local betatron wavelength can significantly mitigate the phase space emittance growth during the vacuum propagation downstream of the plasma cell [33]. The tailored profile was obtained from an OpenFOAM simulation based on a realistic geometry for a plasma cell. The total length of the profiles, shown in Fig. 1, is 80 mm for both cases. When limiting the profile

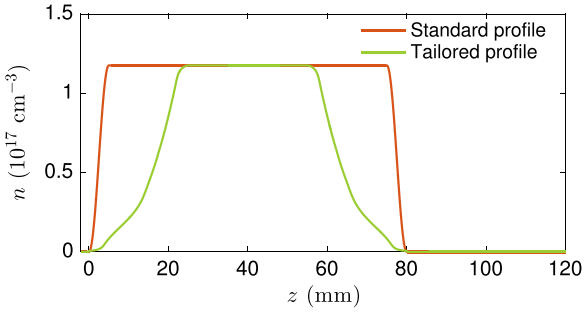

Fig. 1. Longitudinal plasma profiles used for the presented study.

by the drive beam energy depletion length, the tailored case in principle allows for longer plasma target, resulting in a final energy comparable to the one obtained in the standard profile. The choice of targets with equal length in this study is to allow for a better comparison of the emittance growth during the vacuum drift downstream the plasma target. The flattop electron density in both cases is $n_0 = 1.176\times 10^{17}$ cm^{-3}.

Inherent with a change of the plasma frequency along the propagation distance is the change of the normalised parameter

$$\hat{k}_x(z) = \frac{d}{dx}(E_x - B_y)\Big|_{x=0} = \frac{\omega_p^2(z)}{2\omega_{p,0}^2} = \frac{n(z)}{2n_0} \tag{19}$$

in Eqs. (16) and (17), where E_x and B_y are normalised to the cold nonrelativistic wavebreaking field $E_0 = \omega_{p,0} m_e c/e$ [34]. The normalised force in longitudinal direction in the blowout regime may be approximated with a linear function with respect to ζ as follows:

$$F_z(\zeta,z) \simeq \frac{n(z)}{n_0}\frac{dEz}{d\zeta}\left(\zeta - \zeta_d - \sqrt{\frac{n_0}{n(z)}}d_b\right) \tag{20}$$

$$= \frac{dEz}{d\zeta}\left(\frac{n(z)}{n_0}(\zeta-\zeta_d) - \sqrt{\frac{n(z)}{n_0}}d_b\right) \tag{21}$$

where $dEz/d\zeta$ is the slope of the longitudinal field with respect to the co-moving position, normalised to $E_0 k_{p,0}$, with values ranging up to 1/2. The co-moving position of the drive beam center is denoted by ζ_d and d_b represents the normalised distance between the center of the drive beam and the zero-crossing of the E_z curve. In this example study all phase space subsets are assumed to be at the same co-moving location. This means, although the presented approach in principle allows us to take an initial energy chirp or the temporal evolution of the energy chirp into account, this effect is neglected in this study for simplicity. Therefore the mean energy is varying while the absolute energy spread is kept constant. The distance between the drive beam center and all witness beam particles is set to $\zeta_w - \zeta_d = 3.5$. The values for the normalised slope of the longitudinal electric field $dEz/d\zeta \approx 0.3$ as well as the normalised distance between drive beam center and zero-crossing of the electric field $d_b \approx 2.45$ in this study are obtained from the PIC simulations. The witness beam in this investigation has an initial uncorrelated Gaussian energy spread, defined by

$$N_k = \frac{1}{\sqrt{2\pi}\sigma_{\gamma,0}}\exp\left(-\frac{(\gamma_k(t=0)-\overline{\gamma}_0)^2}{2\sigma_{\gamma,0}^2}\right) \tag{22}$$

with the initial energy of the beam $\overline{\gamma}_0 = 2000$ and the initial relative energy spread $\sigma_{\gamma,0}/\gamma = 0.1$. The number of subsets is set to $M=50$ for this study and all subsets are located at the same co-moving position $\zeta_k \equiv \zeta_w \forall k$. The initial transverse beam parameters at the position $z_0 = -2$ mm are chosen as $\sqrt{\langle x^2\rangle_0} = 2$ μm, $\langle x p_x\rangle_0 = 0$ and $\epsilon_0 = 1$ μm. The initial momentum spread in this case can be calculated through $\sqrt{\langle p_x^2\rangle_0} = \epsilon_0/\sqrt{\langle x^2\rangle_0}$.

The particle-in-cell simulations in this work are performed with the 3D quasi-static PIC code HiPACE [21]. The beam parameters as well as the plasma profiles in the PIC simulations are identical to the ones used above for the SANA model. The plasma target starts at $z_1 = 0$ mm and end at $z_2 = 80$ mm. The numerical simulation parameters are defined as follows. The simulation box size is $12\times 14\times 14 k_{p,0}^{-3}$, the number of grid points $512\times 256\times 256$ and the time step size is $dt = 3.0\omega_{p,0}^{-1}$. The drive beam was initialised with 8 macro-particles per cell and the witness beam with a total number of 10^5 macro-particles. For the plasma, 9 macro-particles per cell were used in the middle of the simulation domain down to 1 macro-particle per cell at the simulation domain boundaries.

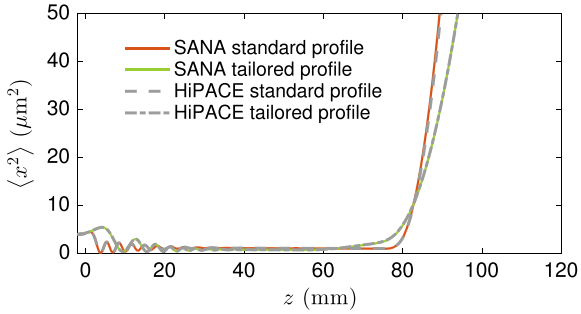

Fig. 2. Evolution of beam envelope moment $\langle x^2 \rangle$ for the standard and tailored longitudinal plasma profile, obtained from SANA and HiPACE. The line legend in this figure applies to all following figures.

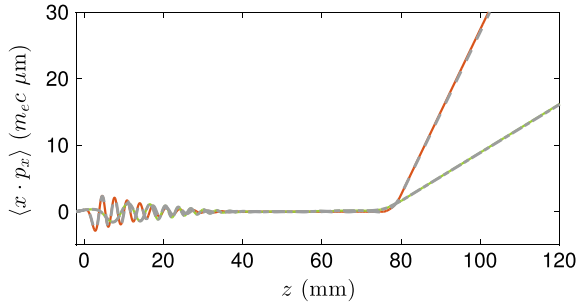

Fig. 3. Evolution of correlation moment $\langle x \cdot p_x \rangle$ for the standard and tailored longitudinal plasma profile, obtained from SANA and HiPACE.

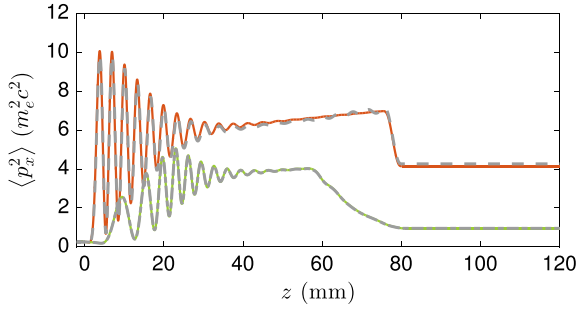

Fig. 4. Evolution of momentum spread moment $\langle p_x^2 \rangle$ for the standard and tailored longitudinal plasma profile, obtained from SANA and HiPACE.

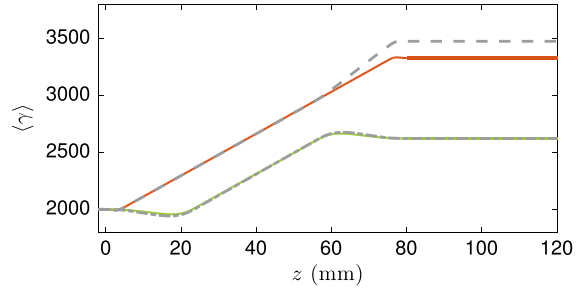

Fig. 5. Evolution of the mean energy $\langle \gamma \rangle$ for the standard and tailored longitudinal plasma profile, obtained from SANA and HiPACE.

The comparisons of the SANA studies and the results obtained from the 3D PIC simulations for the two profiles are depicted in Figs. 2–6. Values in the plots are given in Si units (in contrast to the normalisation in Section 2). Fig. 2 shows the square of the rms beam envelope $\langle x^2 \rangle$. The beam envelopes oscillate during the injection into the plasma wakefield stage according to Eq. (6) if not matched (compare [13]). The various subsets oscillate at slightly different frequencies according to (15) due to the varying energy. This results in a decoherence of the oscillations of the different

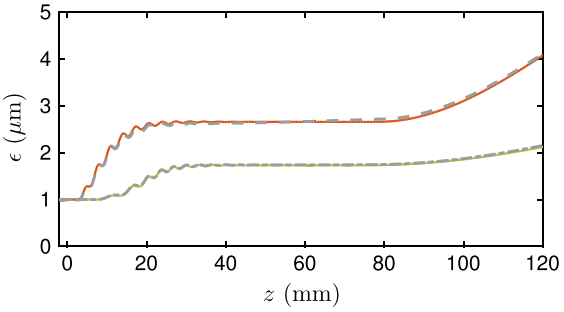

Fig. 6. Emittance evolution for the standard and tailored longitudinal plasma profile, obtained from SANA and HiPACE.

subsets and thereby in a damping of the overall beam envelope in Fig. 2 towards the matched values. The same effect results in the damping of the oscillations for the correlation moment $\langle x \cdot p_x \rangle$ curves in Fig. 3 and the momentum variance $\langle p_x^2 \rangle$ curves in Fig. 4. After full decoherence, the beam is at waist, with $\langle x \cdot p_x \rangle \approx 0$ in Fig. 3. During the propagation in the plasma target, $\langle x^2 \rangle$ decreases adiabatically while $\langle p_x^2 \rangle$ increases adiabatically due to the energy gain of the beam. After traversing the plasma-to-vacuum transition, the beams expand freely in vacuum with $\langle x^2 \rangle$ increasing approximately quadratically, $\langle x \cdot p_x \rangle$ increasing approximately linearly and $\langle p_x^2 \rangle$ remaining constant (cf. [14]). It can be seen qualitatively in Figs. 2–4 that the divergence of the beam exiting the tailored profile is much smaller than the divergence exiting the standard profile. The mean energy, shown in Fig. 5, decreases shortly during the vacuum-to-plasma transition when the witness beam is in the decelerating phase of the plasma wave. Subsequently the energy increases approximately at a constant rate while the energy decreases slightly again during the plasma-to-vacuum transition for the aforementioned reason. The energy gain in the tailored profile is less than in the standard profile. As described before, this stems from the fact that the tailored profile is chosen shorter than in principle allowed by the drive beam energy depletion length. This is to allow for a better comparison of the emittance growth in the tailored and standard cases. The emittance evolution, depicted in Fig. 6, shows the growth during the injection owing to the betatron decoherence (compare [12,13]) and the growth after the beam exits the plasma targets during the expansion in vacuum (compare [14,15]). It can be seen that the emittance growth during the injection is reduced in the tailored plasma profile and the growth rate during the vacuum drift is significantly mitigated in this profile.

When comparing the results from the semi-analytical numerical approach and from the 3D PIC simulations, the curves for the relevant quantities in Figs. 2–6 show an excellent agreement for all relevant quantities. Minor differences between SANA and PIC, especially for the standard profile case, can be attributed to the limited accuracy of the energy gain via Eq. (20). Dominating differences in the energy evolution in Fig. 5 are related to the two following effects taken into account in the PIC simulation but not in the SANA results. Firstly, the resonance or non-resonance of the wake excitation at different plasma densities, modelled in the PIC method results in the differences of the SANA and PIC curves during the slow transitions in the tailored profile. Secondly, and more apparent is the phenomenon in the PIC simulation of PWFA with the standard profile that the nonlinear wavelength of the plasma wave reduces as the drive beam erodes towards the end of the plasma target. This means that the witness beam is by then placed at a plasma wave phase with more enhanced longitudinal field, such that the energy gain increases. It should be noted that the PIC simulations require on the order of $\sim 10^3$ CPU hours,

whereas the computation by means of the SANA method requires only on the order of $\sim 10^{-2}$ CPU hours.

4. Summary and conclusion

This paper presents a semi-analytical numerical approach, which models relevant phase space moments of beams in PWFA much more efficiently than PIC simulations. Such an approach allows for the rapid optimisation of beam parameters and the longitudinal plasma profile in order to preserve the transverse beam quality during the injection and extraction from and into the plasma cell, respectively. The accuracy of the method is demonstrated by comparison of results to those obtained from a PIC simulation, showing excellent agreement. In addition, this work indicates that the dramatic emittance growth during the beam injection into the plasma target and beam expansion downstream of the plasma target can significantly be reduced by tailoring of the longitudinal plasma profile.

Acknowledgements

We acknowledge the use of the High-Performance Cluster (IT-HPC) at DESY. This work was funded in part by the Humboldt Professorship of B. Foster, the DAAD, the Helmholtz Virtual Institute VH-VI-503 and ARD program. The work is part of EuCARD-2, partly funded by the European Commission, GA 312453.

References

[1] I. Blumenfeld, C.E. Clayton, F.-J. Decker, M.J. Hogan, C. Huang, R. Ischebeck, R. Iverson, C. Joshi, T. Katsouleas, N. Kirby, W. Lu, K.A. Marsh, W.B. Mori, P. Muggli, E. Oz, R.H. Siemann, D. Walz, M. Zhou, Nature 445 (7129) (2007) 741, http://dx.doi.org/10.1038/nature05538.

[2] V.I. Veksler, Coherent principle of acceleration of charged particles, in: Proceedings of the CERN Symposium On High-Energy Accelerators and Pion Phyiscs, 1956, pp. 80–83, URL ⟨http://inspirehep.net/record/921325?ln=en⟩.

[3] P. Chen, J.M. Dawson, R.W. Huff, T. Katsouleas, Physical Review Letters 54 (1985) 693, http://dx.doi.org/10.1103/PhysRevLett.54.693, URL ⟨http://link.aps.org/doi/10.1103/PhysRevLett.54.693⟩.

[4] M. Litos, E. Adli, W. An, C.I. Clarke, C.E. Clayton, S. Corde, J.P. Delahaye, R.J. England, A.S. Fisher, J. Frederico, S. Gessner, S.Z. Green, M.J. Hogan, C. Joshi, W. Lu, K.A. Marsh, W.B. Mori, P. Muggli, N. Vafaei-Najafabadi, D. Walz, G. White, Z. Wu, V. Yakimenko, G. Yocky, Nature 515 (7525) (2014) 92, http://dx.doi.org/10.1038/nature13882, URL ⟨http://dx.doi.org/10.1038/nature13882⟩.

[5] A. Seryi, M. Hogan, S. Pei, T. Raubenheimer, P. Tenenbaum, T. Katsouleas, C. Huang, C. Joshi, W. Mori, P. Muggli, A concept of plasma wake field acceleration linear collider (PWFA-LC) WE6PFP081, URL ⟨http://www.slac.stanford.edu/cgi-wrap/getdoc/slac-pub-13766.pdf⟩, 2010.

[6] H. Suk, N. Barov, J.B. Rosenzweig, E. Esarey, Physical Review Letters 86 (2001) 1011, http://dx.doi.org/10.1103/PhysRevLett.86.1011, URL ⟨http://link.aps.org/doi/10.1103/PhysRevLett.86.1011⟩.

[7] E. Oz, S. Deng, T. Katsouleas, P. Muggli, C.D. Barnes, I. Blumenfeld, F.J. Decker, P. Emma, M.J. Hogan, R. Ischebeck, R.H. Iverson, N. Kirby, P. Krejcik, C. O'Connell, R.H. Siemann, D. Walz, D. Auerbach, C.E. Clayton, C. Huang, D.K. Johnson, C. Joshi, W. Lu, K.A. Marsh, W.B. Mori, M. Zhou, Physical Review Letters 98 (2007) 084801, http://dx.doi.org/10.1103/PhysRevLett.98.084801, URL ⟨http://link.aps.org/doi/10.1103/PhysRevLett.98.084801⟩.

[8] J. Vieira, S.F. Martins, V.B. Pathak, R.A. Fonseca, W.B. Mori, L.O. Silva, Physical Review Letters 106 (2011) 225001, http://dx.doi.org/10.1103/PhysRevLett.106.225001, URL ⟨http://link.aps.org/doi/10.1103/PhysRevLett.106.225001⟩.

[9] B. Hidding, G. Pretzler, J.B. Rosenzweig, T. Königstein, D. Schiller, D.L. Bruhwiler, Physical Review Letters 108 (2012) 035001, http://dx.doi.org/10.1103/PhysRevLett.108.035001, URL ⟨http://link.aps.org/doi/10.1103/PhysRevLett.108.035001⟩.

[10] F. Li, J.F. Hua, X.L. Xu, C.J. Zhang, L.X. Yan, Y.C. Du, W.H. Huang, H.B. Chen, C.X. Tang, W. Lu, C. Joshi, W.B. Mori, Y.Q. Gu, Physical Review Letters 111 (2013) 015003, http://dx.doi.org/10.1103/PhysRevLett.111.015003, URL ⟨http://link.aps.org/doi/10.1103/PhysRevLett.111.015003⟩.

[11] A. Martinez de la Ossa, J. Grebenyuk, T. Mehrling, L. Schaper, J. Osterhoff, Physical Review Letters 111 (2013) 245003, http://dx.doi.org/10.1103/PhysRevLett.111.245003, URL ⟨http://link.aps.org/doi/10.1103/PhysRevLett.111.245003⟩.

[12] P. Michel, C.B. Schroeder, B.A. Shadwick, E. Esarey, W.P. Leemans, Physical Review E 74 (2006) 026501, http://dx.doi.org/10.1103/PhysRevE.74.026501, URL ⟨http://link.aps.org/doi/10.1103/PhysRevE.74.026501⟩.

[13] T. Mehrling, J. Grebenyuk, F.S. Tsung, K. Floettmann, J. Osterhoff, Physical Review Special Topics—Accelerators and Beams 15 (2012) 111303, http://dx.doi.org/10.1103/PhysRevSTAB.15.111303, URL ⟨http://link.aps.org/doi/10.1103/PhysRevSTAB.15.111303⟩.

[14] K. Floettmann, Physical Review Special Topics—Accelerators and Beams 6 (2003) 034202, http://dx.doi.org/10.1103/PhysRevSTAB.6.034202, URL ⟨http://link.aps.org/doi/10.1103/PhysRevSTAB.6.034202⟩.

[15] M. Migliorati, A. Bacci, C. Benedetti, E. Chiadroni, M. Ferrario, A. Mostacci, L. Palumbo, A.R. Rossi, L. Serafini, P. Antici, Physical Review Special Topics—Accelerators and Beams 16 (2013) 011302, http://dx.doi.org/10.1103/PhysRevSTAB.16.011302, URL ⟨http://link.aps.org/doi/10.1103/PhysRevSTAB.16.011302⟩.

[16] R. Assmann, K. Yokoya, Nuclear Instruments and Methods in Physics Research Section A: Accelerators, Spectrometers, Detectors and Associated Equipment 410 (3) (1998) 544, http://dx.doi.org/10.1016/S0168-9002(98)00187-9, URL ⟨http://www.sciencedirect.com/science/article/pii/S0168900298001879⟩.

[17] K. Marsh, C. Clayton, D. Johnson, C. Huang, C. Joshi, W. Lu, W. Mori, M. Zhou, C. Barnes, F.-J. Decker, M. Hogan, R. Iverson, P. Krejcik, C. O'Connell, R. Siemann, D. Walz, S. Deng, T. C. Katsouleas, P. Muggli, E. Oz, Beam matching to a plasma wake field accelerator using a ramped density profile at the plasma boundary, in: Proceedings of the Particle Accelerator Conference, PAC 2005, 2005, pp. 2702–2704, http://dx.doi.org/10.1109/PAC.2005.1591234.

[18] K. Floettmann, Physical Review Special Topics—Accelerators and Beams 17 (2014) 054402, http://dx.doi.org/10.1103/PhysRevSTAB.17.054402, URL ⟨http://link.aps.org/doi/10.1103/PhysRevSTAB.17.054402⟩.

[19] I. Dornmair, K. Floettmann, A.R. Maier, Physical Review Special Topics—Accelerators and Beams 18 (2015) 041302, http://dx.doi.org/10.1103/PhysRevSTAB.18.041302, URL ⟨http://link.aps.org/doi/10.1103/PhysRevSTAB.18.041302⟩.

[20] R. Robson, T. Mehrling, J. Osterhoff, Annals of Physics 356 (2015) 306, http://dx.doi.org/10.1016/j.aop.2015.03.004, URL ⟨http://www.sciencedirect.com/science/article/pii/S0003491615000998⟩.

[21] T. Mehrling, C. Benedetti, C.B. Schroeder, J. Osterhoff, Plasma Physics and Controlled Fusion 56 (8) (2014) 084012, URL ⟨http://stacks.iop.org/0741-3335/56/i=8/a=084012⟩.

[22] A. Vlasov, Journal of Physics USSR 9 (1945) 25.

[23] W. Lu, C. Huang, M. Zhou, W.B. Mori, T. Katsouleas, Physical Review Letters 96 (2006) 165002, http://dx.doi.org/10.1103/PhysRevLett.96.165002, URL ⟨http://link.aps.org/doi/10.1103/PhysRevLett.96.165002⟩.

[24] P. Bertrand, A. Ghizzo, T.W. Johnston, M. Shoucri, E. Fijalkow, M.R. Feix, Physics of Fluids B 2 (5) (1990) 1028, http://dx.doi.org/10.1063/1.859276, URL ⟨http://scitation.aip.org/content/aip/journal/pofb/2/5/10.1063/1.859276⟩.

[25] J. Krall, G. Joyce, E. Esarey, Physical Review A 44 (1991) 6854, http://dx.doi.org/10.1103/PhysRevA.44.6854, URL ⟨http://link.aps.org/doi/10.1103/PhysRevA.44.6854⟩.

[26] M. Shoucri, Communications in Computational Physics 4 (3) (2008) 703.

[27] R. Hockney, J. Eastwood, Computer Simulation Using Particles, Advanced Book Program: Addison-Wesley, McGraw-Hill, New York, 1981.

[28] J.M. Dawson, Reviews of Modern Physics 55 (1983) 403, http://dx.doi.org/10.1103/RevModPhys.55.403, URL ⟨http://link.aps.org/doi/10.1103/RevModPhys.55.403⟩.

[29] C. Birdsall, A. Langdon, Plasma Physics via Computer Simulation, The Adam Hilger Series on Plasma Physics, McGraw-Hill, New York, 1985.

[30] K. Kumar, Journal of Physics D: Applied Physics 14 (12) (1981) 2199, URL ⟨http://stacks.iop.org/0022-3727/14/i=12/a=008⟩.

[31] M. Reiser, Theory and Design of Charged Particle Beams, Wiley Series in Beam Physics and Accelerator Technology, John Wiley & Sons, New York, 2008.

[32] E. Esarey, B.A. Shadwick, P. Catravas, W.P. Leemans, Physical Review E 65 (2002) 056505, http://dx.doi.org/10.1103/PhysRevE.65.056505, URL ⟨http://link.aps.org/doi/10.1103/PhysRevE.65.056505⟩.

[33] T.J. Mehrling, Theoretical and numerical studies on the transport of transverse beam quality in plasma-based accelerators (Ph.D. thesis), Universitt Hamburg, Von-Melle-Park 3, 20146 Hamburg, 2014, URL ⟨http://ediss.sub.uni-hamburg.de/volltexte/2014/7029⟩.

[34] J.M. Dawson, Physical Review 113 (1959) 383, http://dx.doi.org/10.1103/PhysRev.113.383, URL ⟨http://link.aps.org/doi/10.1103/PhysRev.113.383⟩.